The Influence of Iodide on the Solution-Phase Growth of Cu Microplates: A Multi-Scale Theoretical Analysis from First Principles

Junseok Kim[1] *and Kristen A. Fichthorn*[1,2]*

Department of Chemical Engineering[1] and Department of Physics[2]; The Pennsylvania State University; University Park, PA 16802 USA

*Email: fichthorn@psu.edu

Contents

Table S1. Cu atom binding energies for sites shown in Figure 5.

Facet	Binding positions	Binding energy (eV)
{111}	1	-3.41
	2	-3.39
	3	-3.54
	4	-3.53
	5	-3.30
	6	-3.44
{100}	7	-3.59
	8	-3.70
	9	-3.71
	10	-3.68

Table S2. Binding energies for the sites in Figure S6

Facet	Binding Position	Binding energy (eV)
{111}	1	-3.57
	2	-3.57
	3	-3.74
	4	-3.81
{100}	5	-3.47
	6	-3.92
	7	-3.86
	8	-3.31

Table S3. Binding energies for the sites in Figure 6

Facet	Binding Position	Binding energy (eV)
Top {111}	1	-3.44
	2	-3.50
	3	-3.36
	4	-3.38
Side {111}	1	-3.44
	2	-3.51
	3	-3.37
	4	-3.37

Table S4. Binding energies for the sites in Figure S7

Facet	Binding Position	Binding energy (eV)
Top {111}	1	-3.37
	2	-3.31
Side {111}	1	-3.38
	2	-3.32

Table S5. Convergence test for the energy (eV) of Cu adatom binding on subsurface-hollow (①) of ½ ML of I-Cu(100) in **Figure 2**, with respect to *k*-point mesh, vacuum spacing, and energy cut-off. Shaded cells show the settings used for calculations in this work. All convergence tests were performed within 0.01 eV.

***k*-point mesh**	5x3x1	6x4x1	7x4x1	8x5x1	5x3x1	5x3x1	5x3x1	5x3x1
Vacuum space in z-direction (Å)	15.0	15.0	15.0	15.0	20.0	18.0	15.0	15.0
Energy Cut-off (eV)	400	400	400	400	400	400	450	500
E_{bind} (eV)	-5.02	-5.03	-5.02	-5.02	-5.02	-5.03	-5.03	-5.02

* For 1/3 ML of I-Cu(111), the convergence test is performed for only *k*-point mesh with 0.01 eV criterion using 400 eV for energy cutoff and 15 Å for vacuum spacing, which yields a (7x5x1) *k*-point mesh as an optimal value.

Table S6. Convergence test for the energy (eV) of Cu adatom binding on hollow (⑦) of {100} on the inter-facet slab in **Figure 5**, with respect to *k*-point mesh, vacuum spacing, and energy cut-off. Shaded cells show the settings used for calculations in this work. All convergence test were performed within 0.01 eV.

***k*-point mesh**	2x1x1	3x1x1	4x1x1	4x2x2	5x1x1	4x1x1	4x1x1	4x1x1
Vacuum space in z-direction (Å)	20.0	20.0	20.0	20.0	20.0	18.0	23.0	15.0
E_{bind} (eV)	-3.58	-3.59	-3.59	-3.59	-3.59	-3.59	-3.59	-3.59

* For the inter-facet slab in **Figure 6**, the convergence test is performed for only *k*-point mesh with 0.01 eV criterion using 400 eV for energy cutoff and 20 Å for vacuum spacing, which yields a (1x4x1) *k*-point mesh as an optimal value.

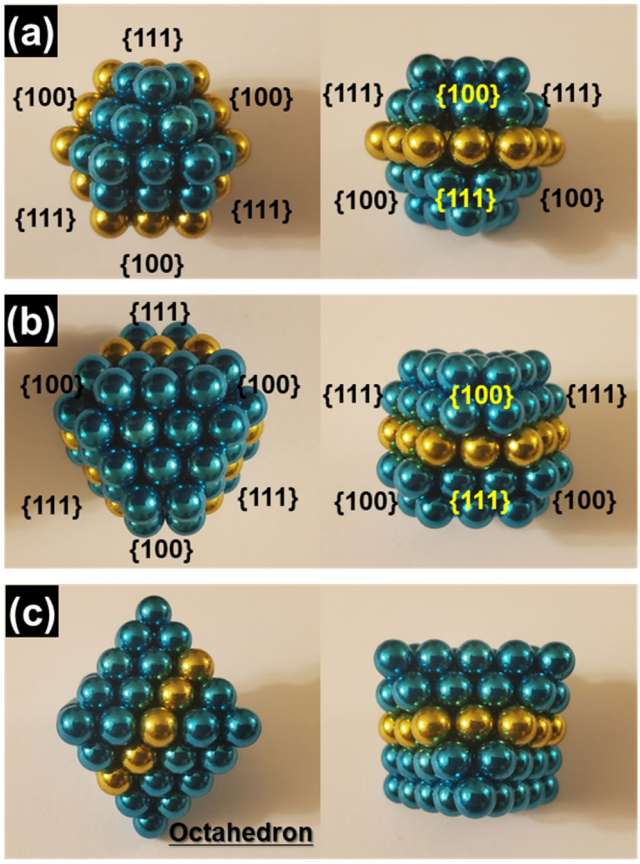

Figure S1. Growth of an hcp plate seed, as a model of a larger plate without stacking fault. A top-down view of a basal facet is shown in the left panel and side view is shown in the right panel. In (a) we show three views of the initial seed, which the alternating facet structure in **Figure 1(a).** In (b) we show the structure after adding an atom to each of the four-fold {100} sites. Subsequent to filling all the {100} sites, we achieve the octahedron structure in (c).

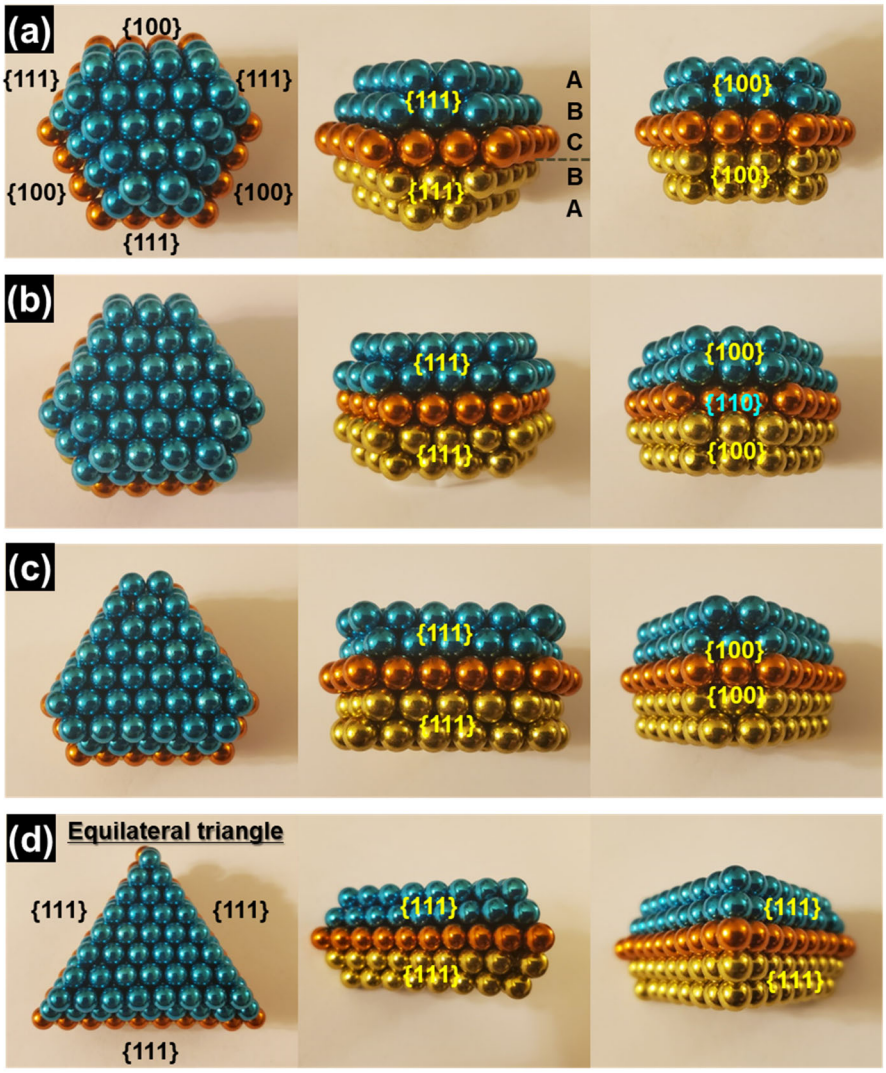

Figure S2. Growth of an hcp plate seed, as a model of a larger plate containing one stacking fault. A top-down view of a basal facet is shown in the left panel and two different side views are shown in the center and right panels. In (a) we show three views of the initial seed, which the mirror-symmetry facet structure in **Figure 1(b).** The center panel indicates the hcp layer stacking. In (b) we show the structure after adding an atom to each of the four-fold {100} sites. Subsequent to filling in all the {100} and {110} sites in (b) and (c), we generate the equilateral triangle, as shown in (d). Further filling of the {111} facets would lead to a trigonal bipyramid.

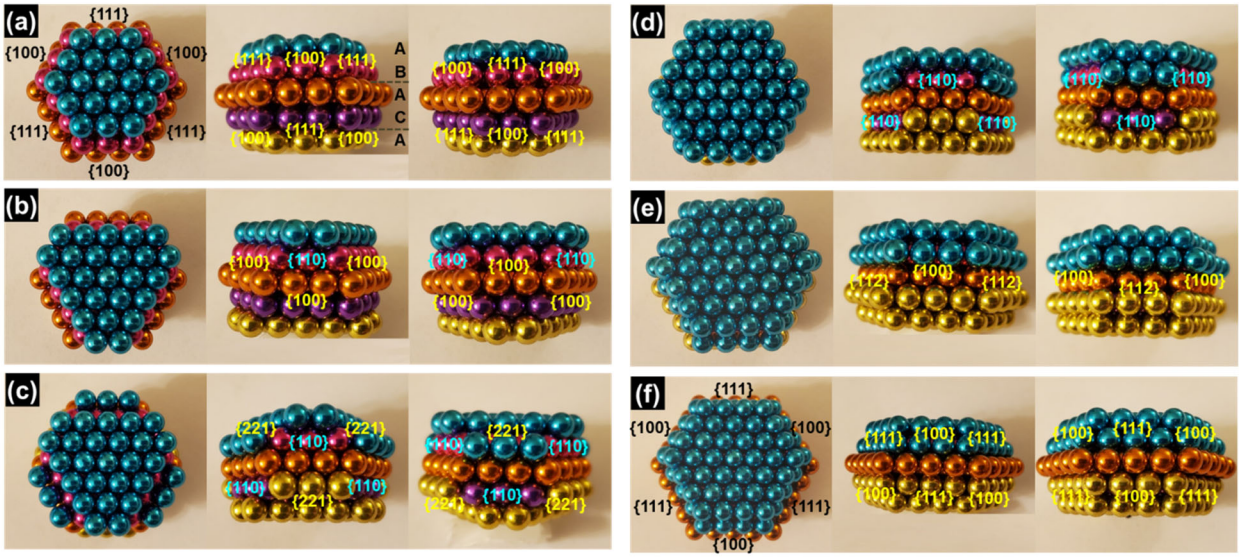

Figure S3. Growth of an hcp plate seed, as a model of a larger plate that we varied the positions of two stacking faults. A top-down view of a basal facet is shown in the left panel and two different side views are shown in the center and right panels. In (a) we show three views of the initial seed, which the alternating facet structure in **Figure 1(a).** The center panel indicates the hcp layer stacking. After filling an atom to each of the four-fold {100} sites in (a) and (b), we attain the structure in (c), where we generated six rows of {221} and {110} sites. Subsequent to filling in all the {221} and {110} sites through (c) to (d), we generate {112} sites newly and regenerate {100} sites in (e). Filling all the {112} and {100} in the middle side produces the hexagonal structure in (f), which regenerates the structure in (a).

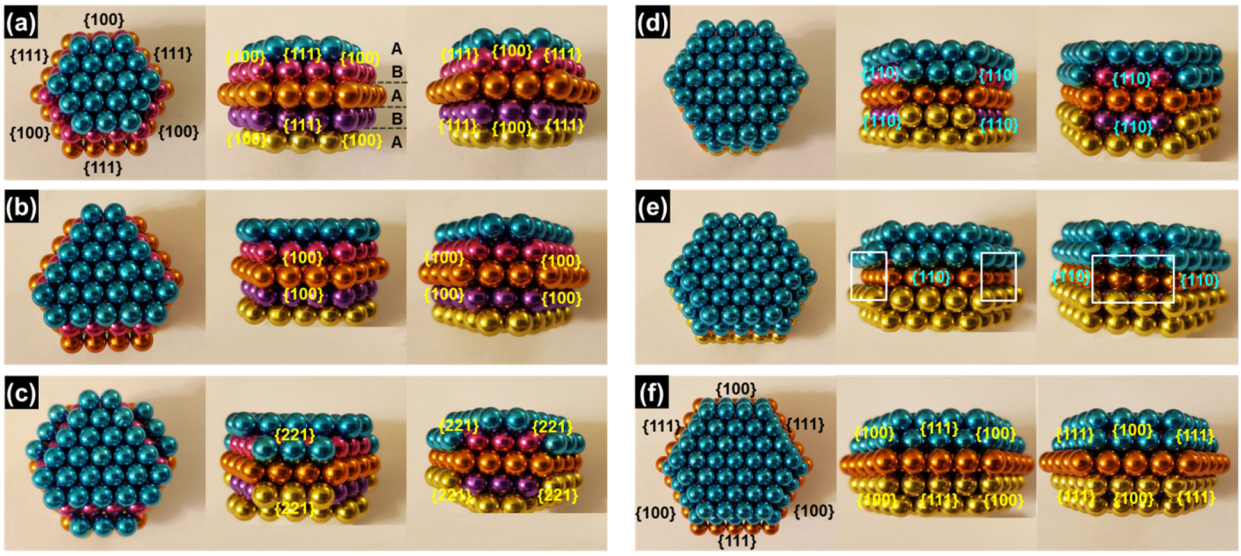

Figure S4. Growth of an hcp plate seed, as a model of a larger plate containing three stacking faults. A top-down view of a basal facet is shown in the left panel and two different side views are shown in the center and right panels. In (a) we show three views of the initial seed, which the mirror-symmetry facet structure in **Figure 1(b).** The center panel indicates the hcp layer stacking. After filling in all the {100}, generated {110} and {221} binding sites, and concave sites (white box) through (b) to (e) as we have done for previous cases, we achieve the hexagonal structure in (f), which regenerates the structure in (a).

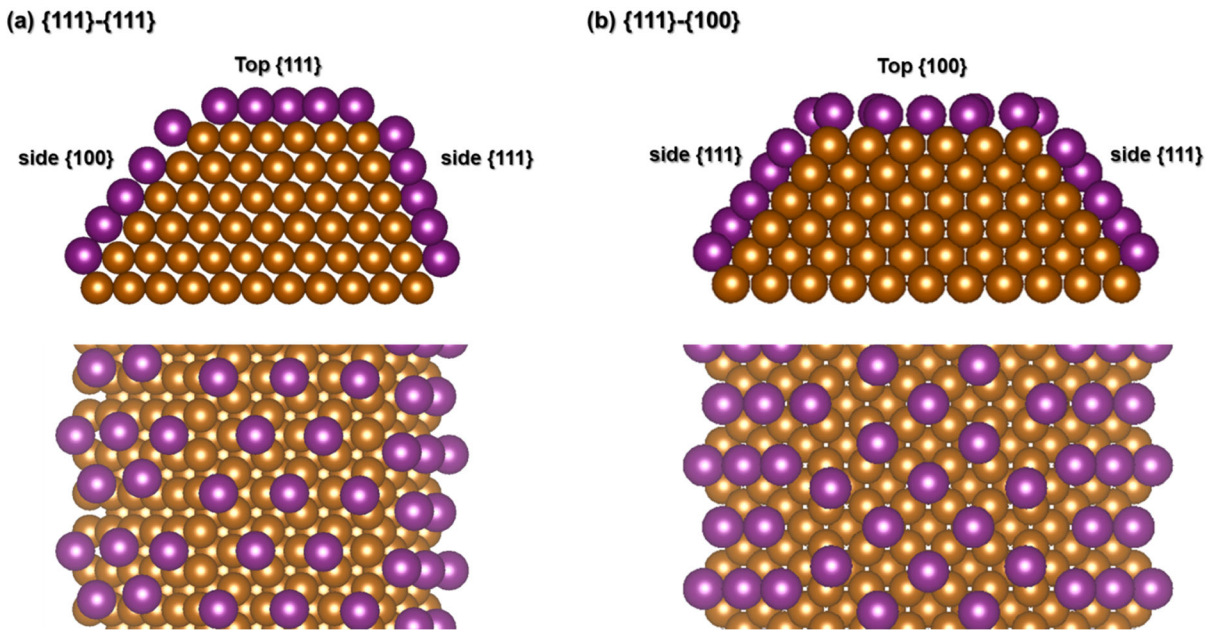

Figure S5. Cu inter-facet slab (a) for {111}-{111} and (b) for {111}-(100}.

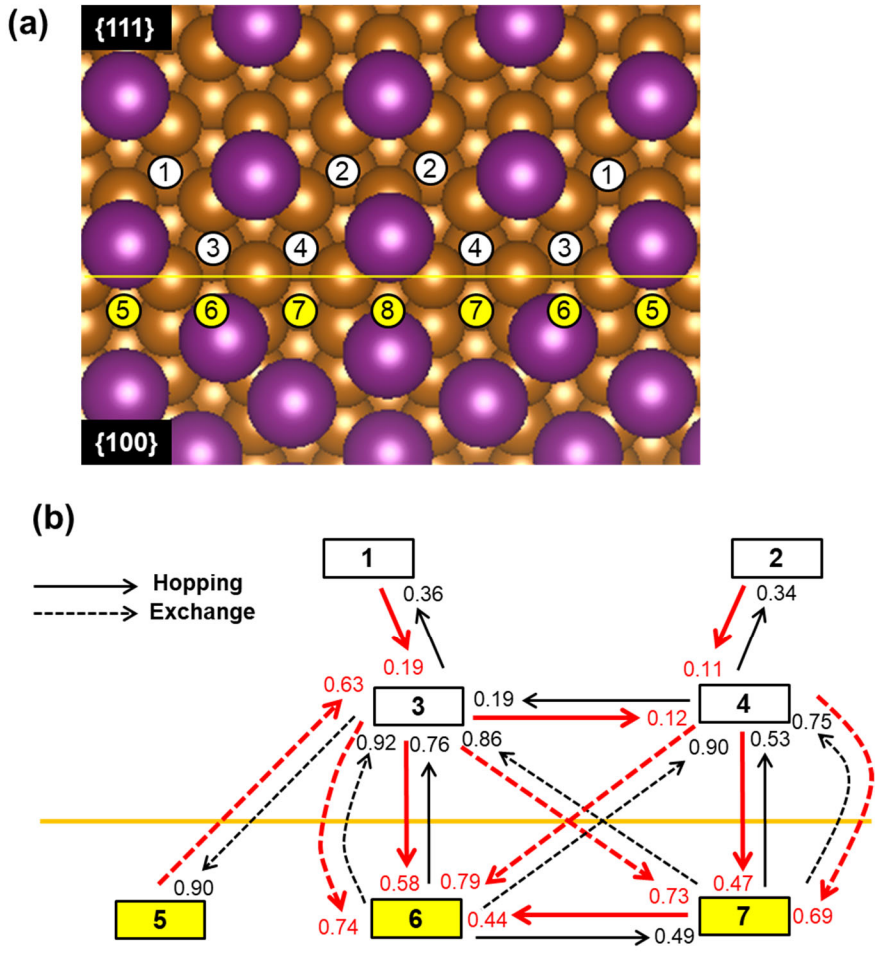

Figure S6. (a) Binding sites for Cu adatom near the {111}-{100} edge when iodine is placed on hcp hollow sites on {111} – viewed from the perpendicular direction to {111} (Cu atoms are orange and I atoms are purple) and (b) the inter-facet diffusion pathways. Numbers at the end of each arrow denote the diffusion energy barrier (in eV) for that pathway. The red arrows denote lower barrier pathways in the forward-reverse pair. Arrows with solid lines represent hopping, while arrows with dashed lines represent exchange diffusion. Hcp{111} binding sites are shown in white and four-fold hollow sites on {100} are shown in yellow.

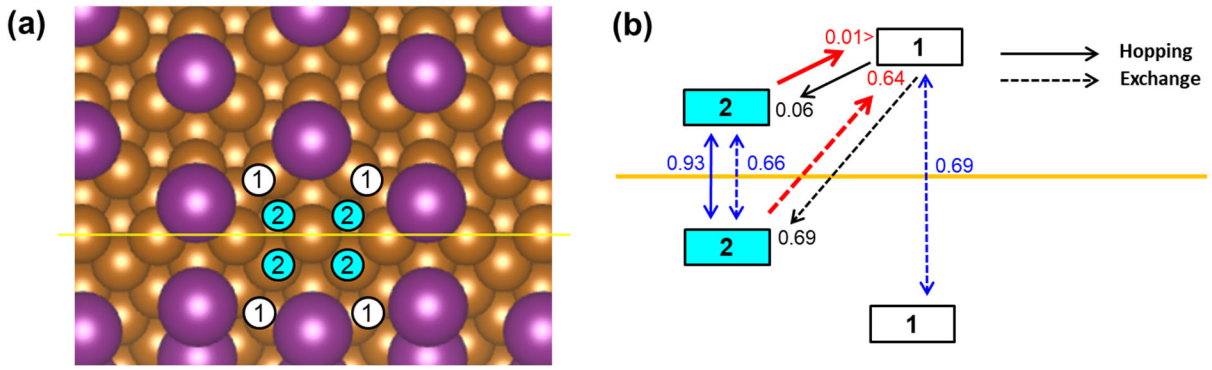

Figure S7. (a) Binding sites for a Cu adatom on the {111}-{111} facet edge when iodine is placed on fcc hollow sites but in a different configuration from **Figure 6** (Cu atoms are orange and I atoms are purple) and (b) inter-facet diffusion pathways. Numbers at the end of each arrow denote the diffusion energy barrier (in eV) for that pathway. The red arrows denote lower barrier pathways in the forward-reverse pair. Arrows with solid lines represent hopping, while arrows with dashed lines represent exchange diffusion. Hcp{111} binding sites are shown in white and fcc{111} binding sites are shown in turquoise.

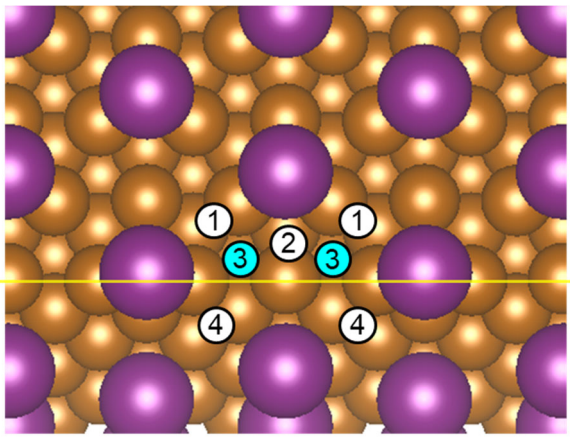

Facet	Binding positions	Binding energy (eV)
Top {111}	1	-3.34
	2	-3.10
	3	-3.32
Side {111}	4	-3.44

Figure S8. Binding sites and corresponding energies for a Cu adatom on the {111}-{111} facet edge when iodine is placed on fcc hollow sites on one facet and hcp on the other. Hcp{111} binding sites are shown in white and fcc{111} binding sites are shown in turquoise.

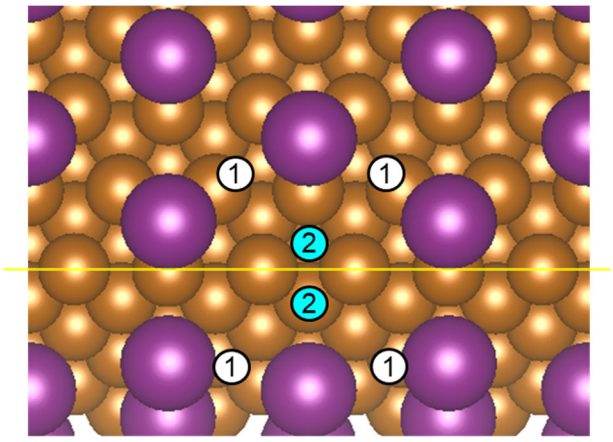

Facet	Binding positions	Binding energy (eV)
Top {111}	1	-3.45
	2	-3.09
Side {111}	1	-3.46
	2	-3.07

Figure S9. Binding sites and corresponding energies for a Cu adatom on the {111}-{111} facet edge when iodine is placed on hcp sites on both facets. Hcp{111} binding sites are shown in white and fcc{111} binding sites are shown in turquoise.

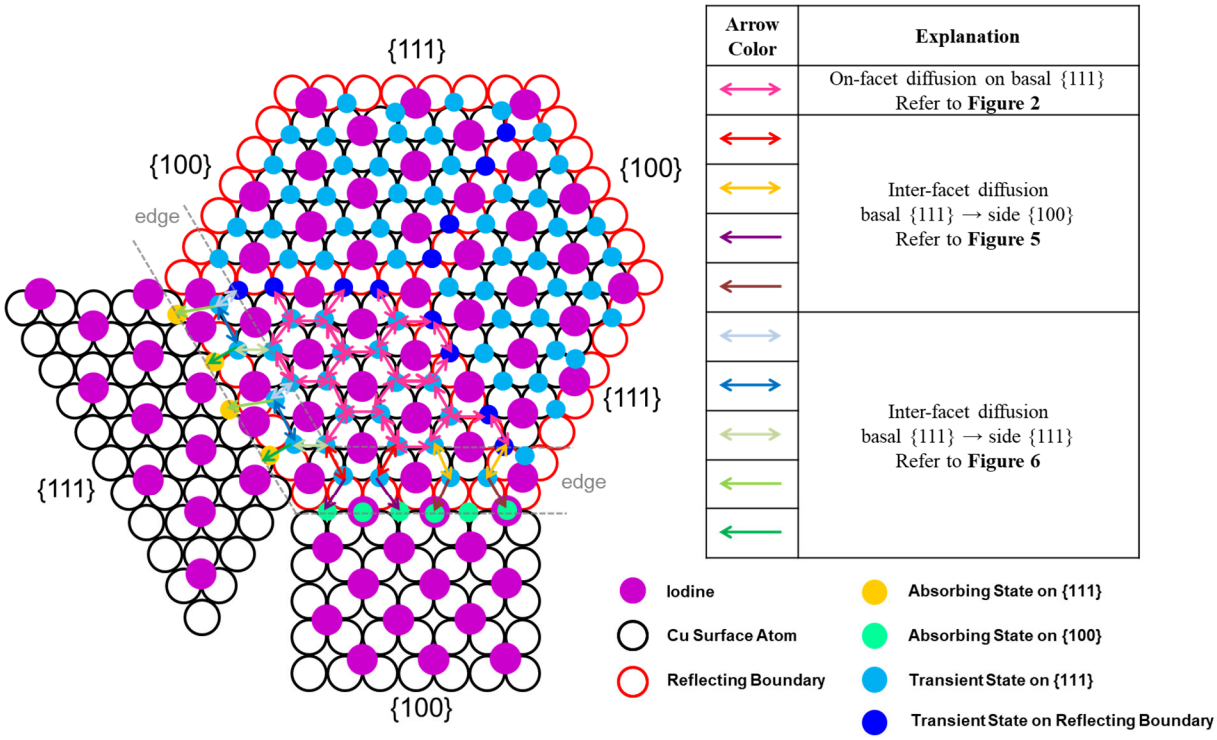

Figure S10. A model for inter-facet diffusion from basal {111} to side {111} and {100} and corresponding barriers between all neighboring sites.

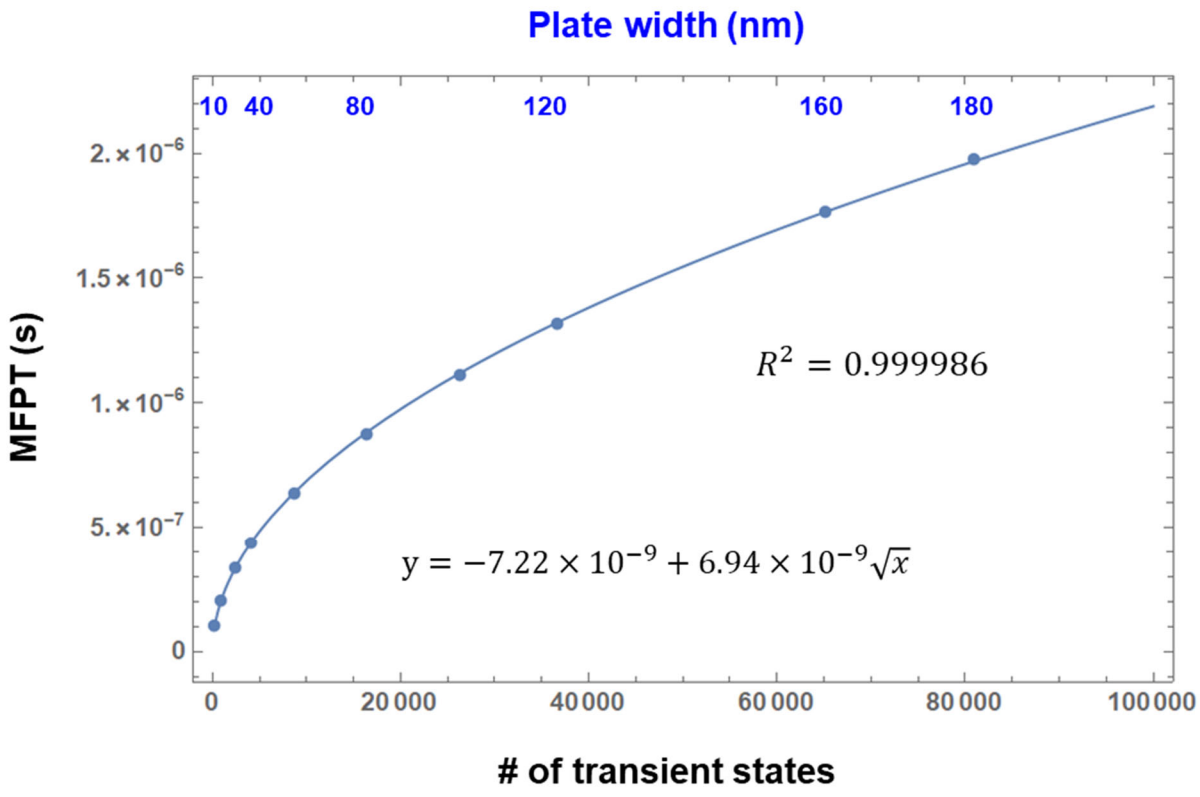

Figure S11. Extrapolation fitting for the MFPT versus the number of transient states that correspond to the plate width.